Supplementary Material (ESI) for Dalton Transactions

Electronic Supplementary Information

Inorganic–organic hybrid materials with different dimensions constructed from copper-fluconazole metal-organic units and Keggin polyanion clusters

Shun-Li Li, Ya-Qian Lan, Jian-Fang Ma,* Jin Yang, Jie Liu, Yao-Mei Fu and Zhong-Min Su

Key Lab of Polyoxometalate Science, *Department of Chemistry*, *Northeast Normal University*, *Changchun 130024*, *People's Republic of China*

* Corresponding author.

E-mail: jianfangma@yahoo.com.cn

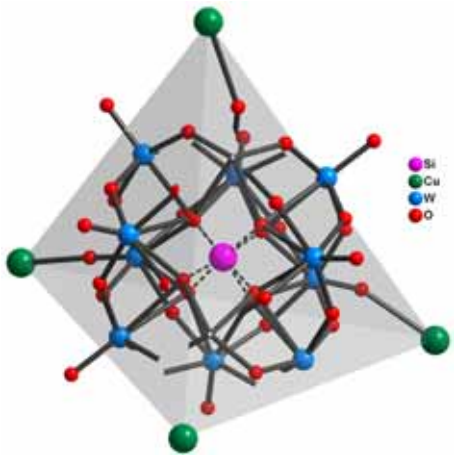

(a)

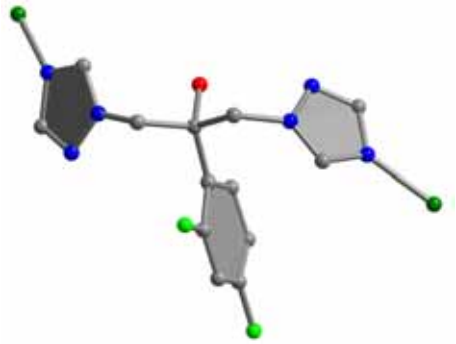

(b)

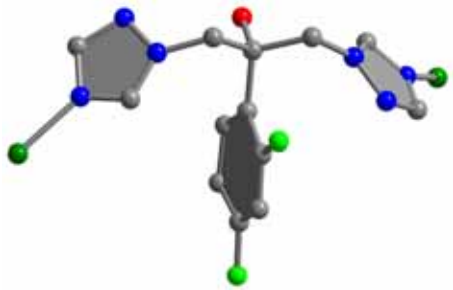

(c)

Fig. S1. (a) Ball-stick representation of coordination mode of the $(SiW_{12}O_{40})^{4-}$ polyoxoanion. (b) and (c) Ball-stick representations of the coordination mode of two kinds of Hfcz ligands.

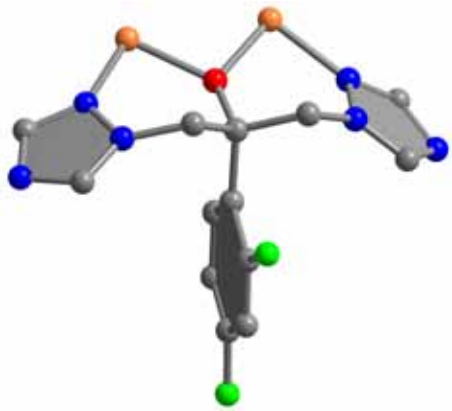

(a)

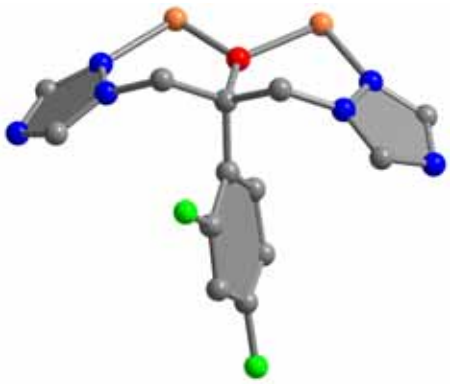

(b)

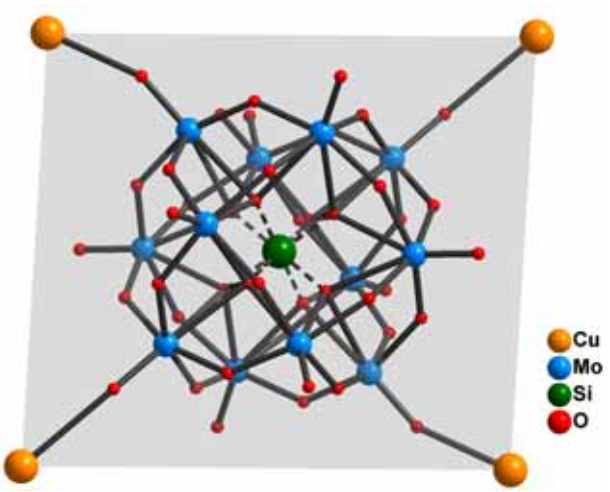

(c)

Fig. S2. (a) and (b) Ball-stick representations of the coordination mode of two kinds of fcz^- ligands. (c) Ball-stick representation of the coordination mode of the $(SiW_{12}O_{40})^{4-}$ polyoxoanion.

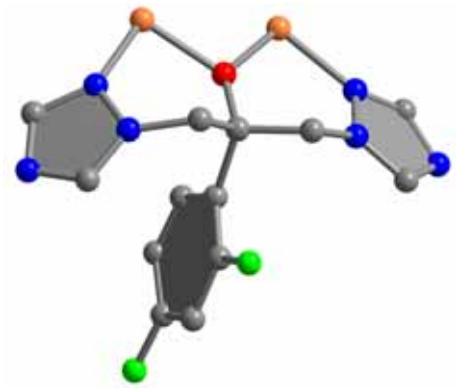

(a)

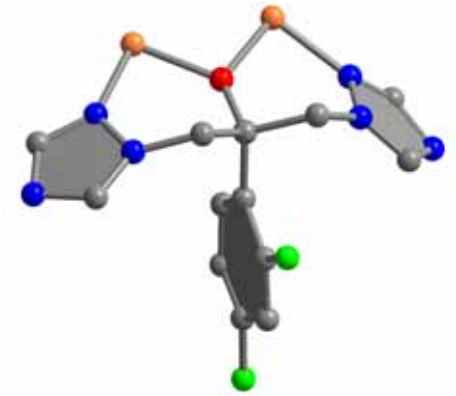

(b)

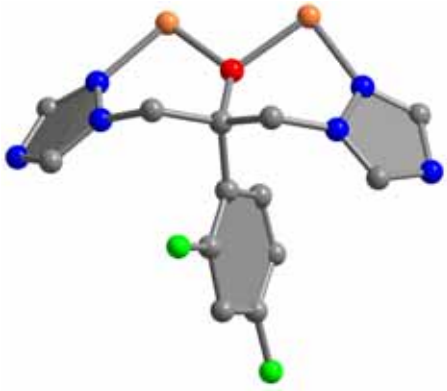

(c)

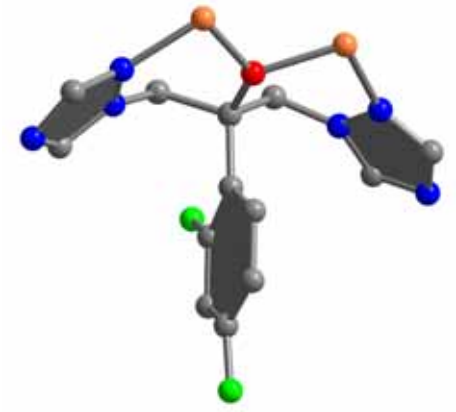

(d)

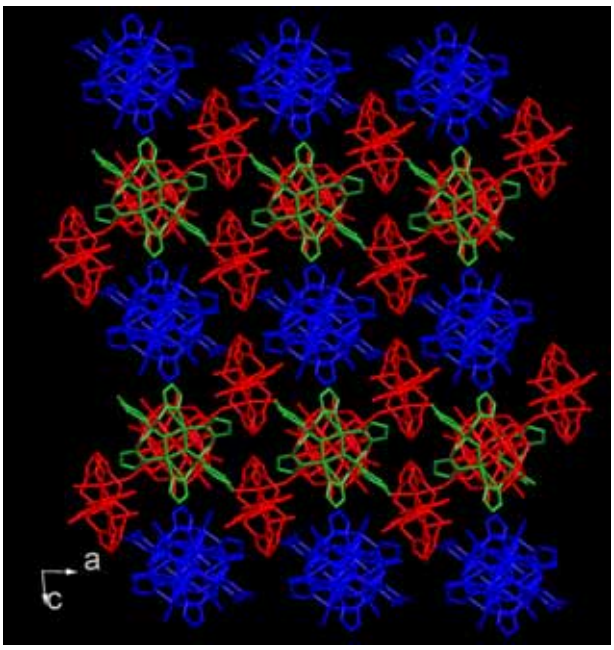

(e)

Fig. S3. (a)-(d) Ball-stick representations of the coordination mode of four kinds of fcz^- ligands. (e) View of the arranged form of three types of isolated subunits in **3** along the *b* axis.

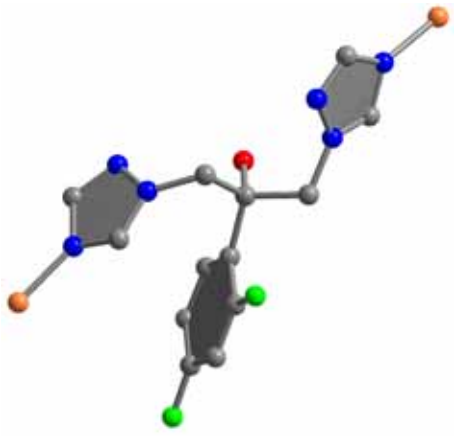

(a)

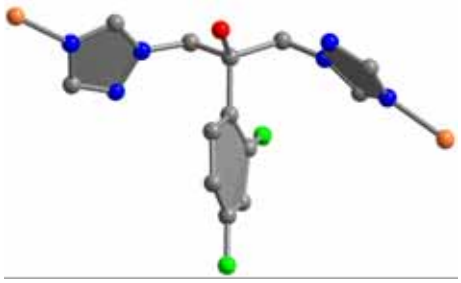

(b)

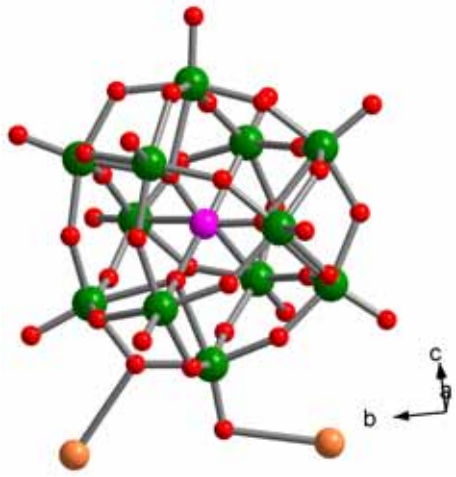

(c)

Fig. S4. (a) and (b) Ball-stick representations of the coordination mode of two kinds of Hfcz ligands. (c) Ball-stick representation of the coordination mode of the $(SiW_{12}O_{40})^{4-}$ anion.

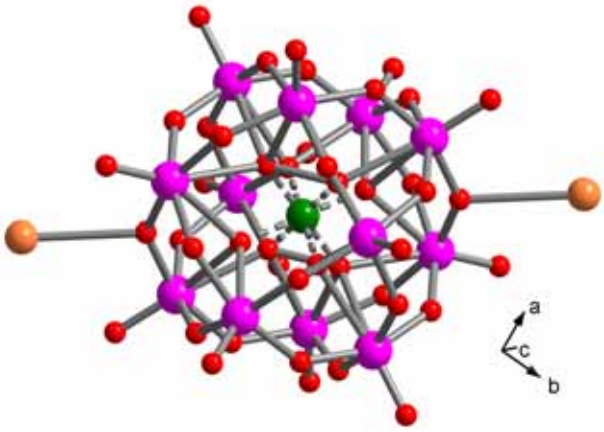

(a)

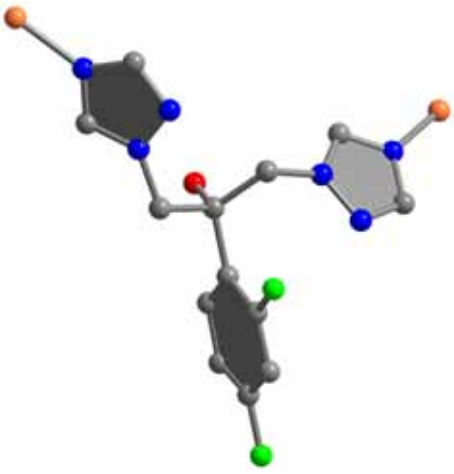

(b)

Fig. S5. (a) Ball-stick representation of the linear coordination mode of the $(SiW_{12}O_{40})^{4-}$ anion. (b) Ball-stick representations of the coordination mode of the Hfcz ligand.

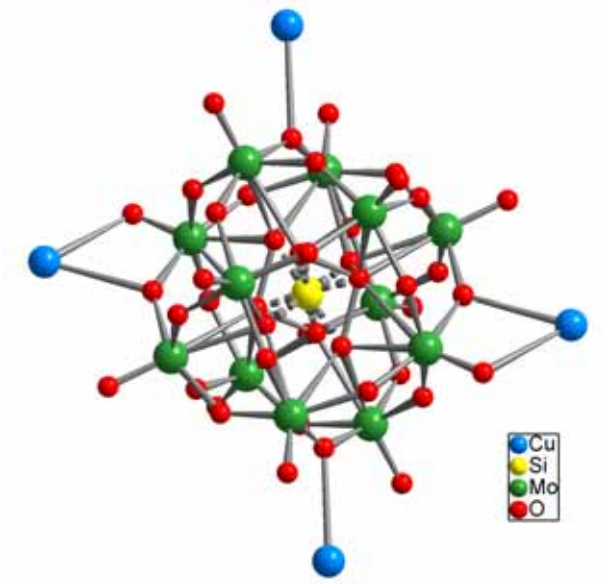

(a)

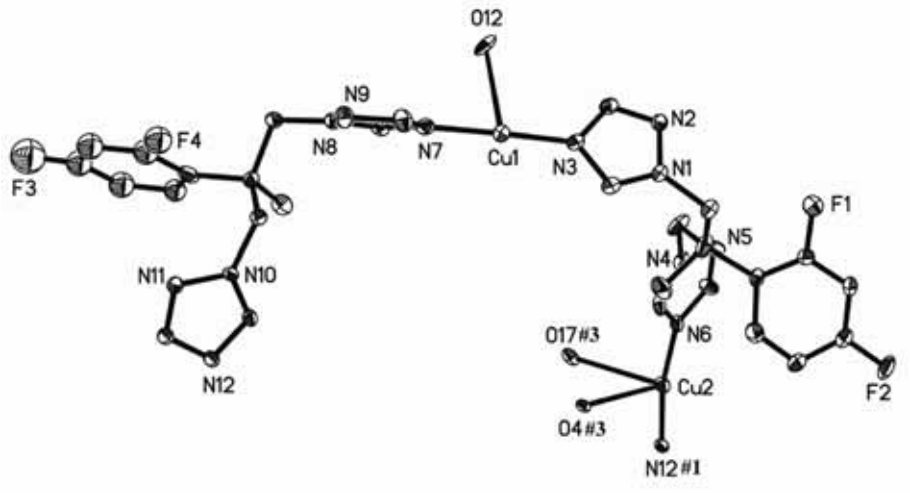

(b)

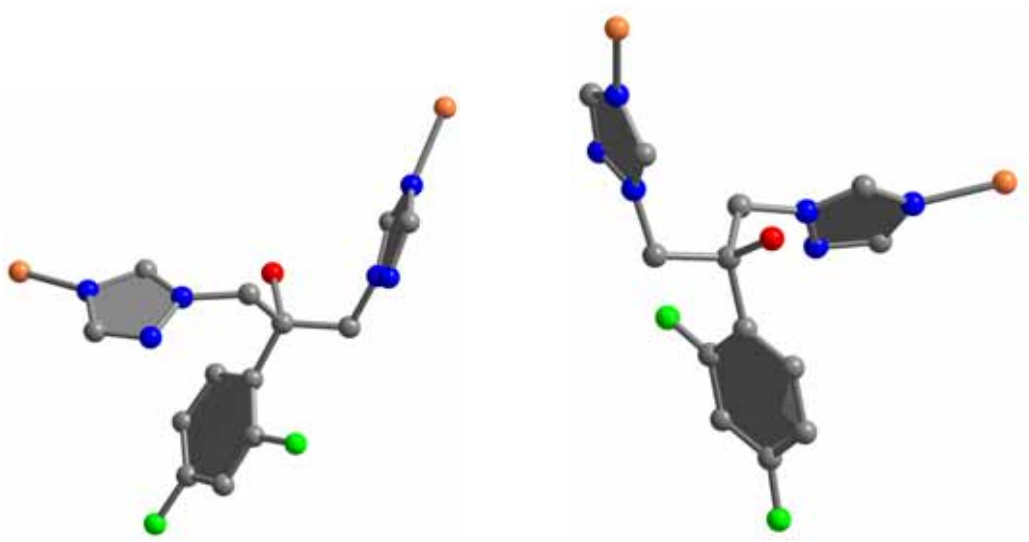

(c) **(d)**

Fig. S6. (a) Ball-stick representation of the coordination mode of the $(SiMo_{12}O_{40})^{4-}$ anion. (b) ORTEP diagram showing the coordination environments for the Cu^{I} atoms in **6**. (c) and (d) Ball-stick representations of the coordination modes of two kinds of Hfcz ligands.

FT-IR Spectroscopy. The IR spectra of compounds **1-6** exhibit four characteristic asymmetric vibrations resulting from the polyanions with the α-Keggin structure. The peak belonging to the M-Ot (M = W and Mo), M–Ob and M–Oc bonds shift from 1000 to 700 cm^{-1}, the Si–O bands appear at 1100-1000 $cm^{-}1$.[1] This shows that the polyanions retain the basic Keggin structure, yet a little distortion due to the coordination influence, and this is in consistent with the result of the single crystal X-ray diffraction analysis. Furthermore, the bands at 3850-3600 cm^{-1} and 1700-1100 cm^{-1} can be attributed to the Hfcz/fcz^{-} ligands.[2]

Thermal Analysis. In order to characterize the compounds more fully in terms of thermal stability, their thermal behaviors were studied by TGA. The experiments were

performed on samples consisting of numerous single crystals of **1**-**6** with a heating rate of 10 °C/min. And the results are shown in Fig. S7. For compound **1**, the weight loss corresponding to the release of water molecules is observed from room temperature to 65 °C (obsd 1.2%, calcd 1.3%). The anhydrous compounds begin to decompose at 310 °C. From room temperature to 102 °C, compound **2** lost its lattice water molecules (obsd 3.3%, calculated 3.1%) and then decomposition of remain occurs at 304 °C. For compound **3**, the weight loss in the range of 42-151 °C corresponds to the departure of water molecules (obsd 1.2%, calcd 1.6%). The removal of the organic components occurs at 314 °C. The TGA curves of **4** and **5** show that they undergo dehydration in the range of 35-118 °C (obsd 1.2%, calcd 0.93%) for **4**, and 40-113 °C (obsd 0.76 %, calcd 0.47 %) for **5**, respectively. Then the decomposition of the anhydrous compound occurs at 311 °C for **4** and 289 °C for **5**. The decomposition of the anhydrous compound **6** occurs at 235 °C.

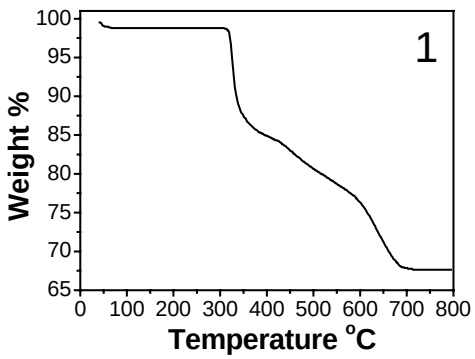

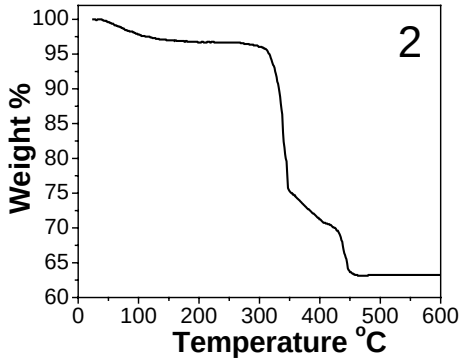

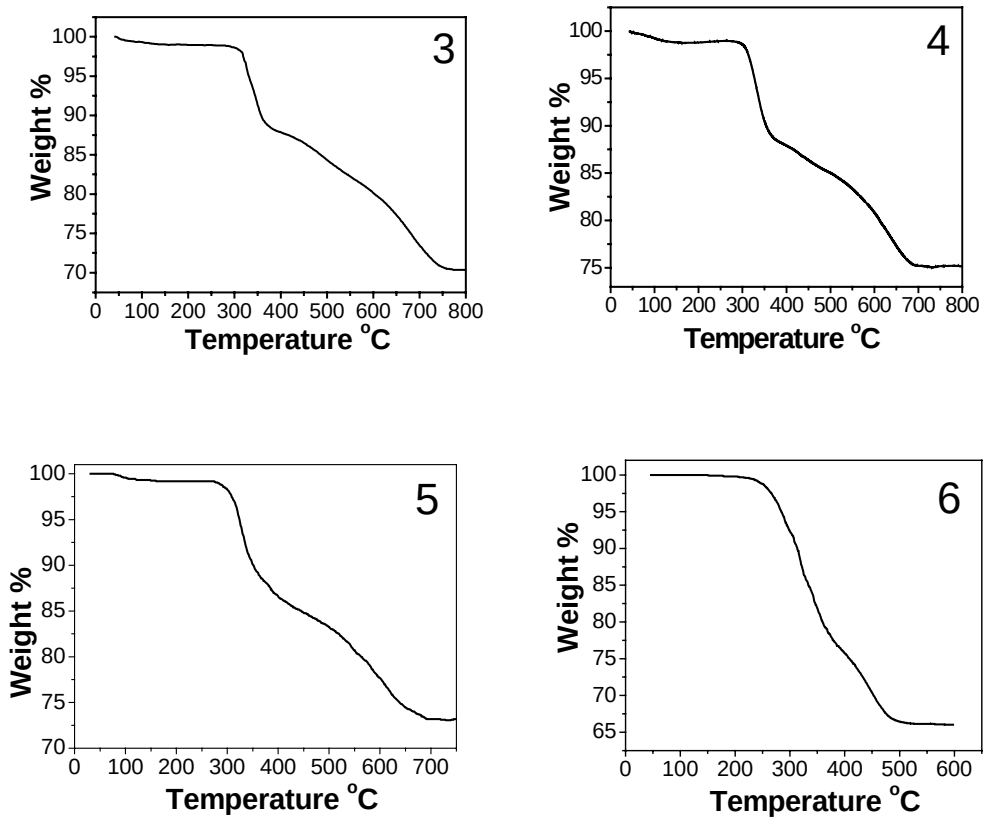

Fig. S7. TGA spectra of compounds **1**-**6**.

Electrochemical Behaviors of the 1-CPE, 2-CPE, 5-CPE and 6-CPE. The electrochemical behaviors of **1**-CPE, **2**-CPE, **5**-CPE and **6**-CPE were studied. Fig. S8 shows the typical cyclic voltammograms at potential range from -700 to 300 mV for **1**-CPE and **5**-CPE, at potential range from -100 to 800 mV for **2**-CPE and **6**-CPE. It can be clearly seen that three reversible redox peaks appear in 1M H_2SO_4 aqueous solution, respectively. Redox peaks I-I', II-II', and III-III' correspond to three consecutive two-electron processes, respectively. The approximate proportionality of the reduction peak current to the scan rate up to 500 mV s^{-1} (Fig. S9) indicates that the redox process is surface-controlled.[3]

In addition, POMs have been employed in electrocatalytic reductions.[4] Here we

investigate the electrocatalytic behaviors of **2**-CPE and **6**-CPE. As shown in Fig. S10, **2**-CPE and **6**-CPE display good electrocatalytic activity toward the reduction of nitrite in 1M H_2SO_4 containing of $NaNO_2$. On addition of NO_2^-, the reduction peak currents increase and the corresponding oxidation peak currents decrease dramatically, and this suggests that nitrite is reduced. The results indicate that the three reduced species all have electrocatalytic activity for nitrite reduction. It was also noted that the third reduced species showed the best electrocatalytic activity, that is, the catalytic activity is enhanced with increasing extent of polyanion reduction.

References:

1 J.-Y. Niu, M.-L. Wei, J.-P. Wang and D.-B. Dang, *Eur. J. Inorg. Chem.*, 2004, 160.

2 (*a*) H. Han, Y. Song, H. Hou, Y. Fan and Y. Zhu, *Dalton Trans.*, 2006, 1972; **(***b*) H. Han, S. Zhang, H. Hou, Y. Fan and Y. Zhu, *Eur. J. Inorg. Chem.*, 2006, 1594; (*c*) S.-L. Li, Y.-Q. Lan, J.-F. Ma, J. Yang, X.-H. Wang and Z.-M. Su, *Inorg. Chem.*, 2007, **46**, 8283.

3 X.-M. Zhang, R.-H. Fang and H.-S. Wu, *J. Am. Chem. Soc.*, 2005, **127**, 7670.

4 (*a*) E. Papaconstantinou, A. Ioannidis, A. Hiskia, P. Argitis, D. Dimoticali, S. Korres, M. T. Pope and A. Müller, (Eds.), *Polyoxometalates: from Platonic Solids to Antiretroviral Activity, Kluwer, Dordrecht,* 1993, 327; *Mol. Eng.* 1993, **3**, 263; (*b*) S. Dong, X. Xi and M. Tian, *J. Electroanal. Chem.*, 1995, **385**, 227; (*c*) B. Keita, A. Belhouari, L. Nadjo and R. Contant, *J. Electroanal. Chem.*, 1995, **381**, 243; (*d*) J. E. Toth and F. C. Anson, *J. Electroanal. Chem.*, 1988, **256**, 361.

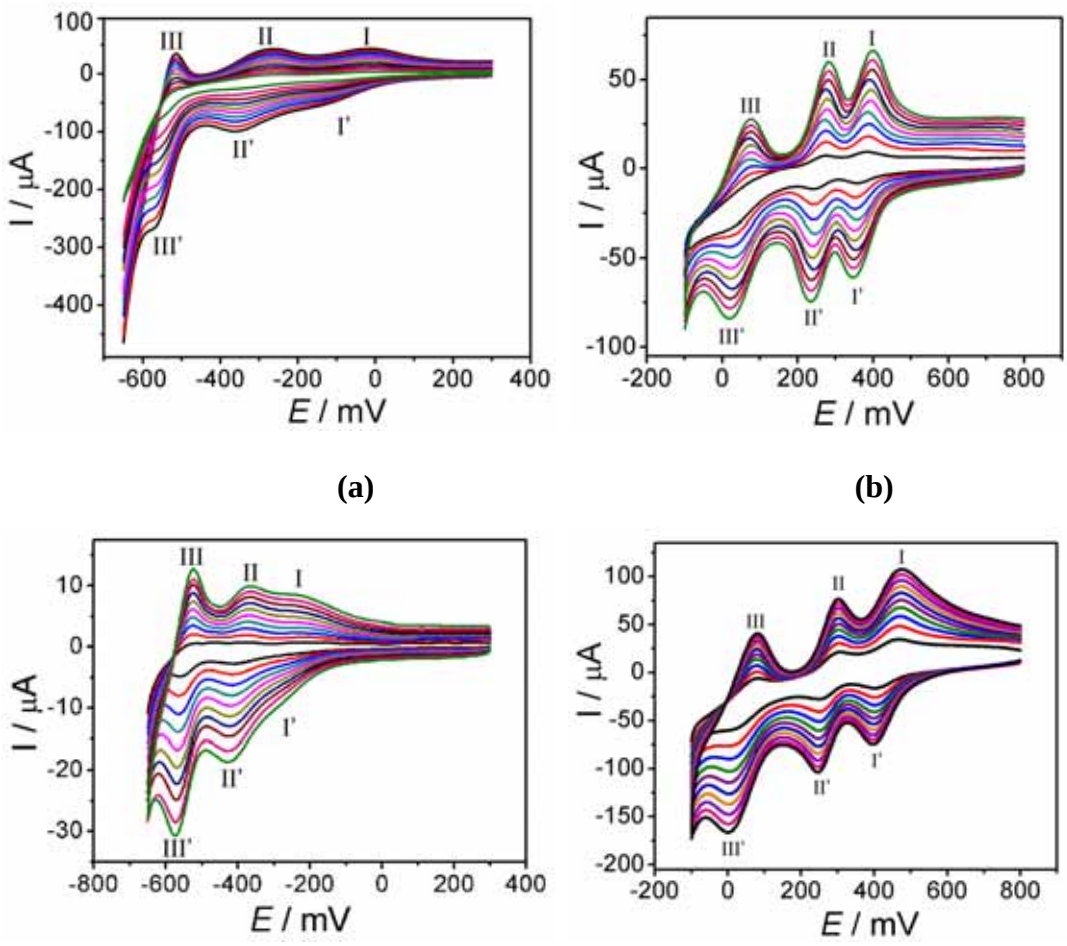

Fig. S8. The cycolic voltammograms of the **1**-CPE (a), **2**-CPE (b), **5**-CPE (c), and **6**-CPE (d) in 1M H_2SO_4 at different scan rates (from inner to outer: 50, 100, 150, 200, 250, 300, 350, 400, 450 and 500 mV s^{-1}).

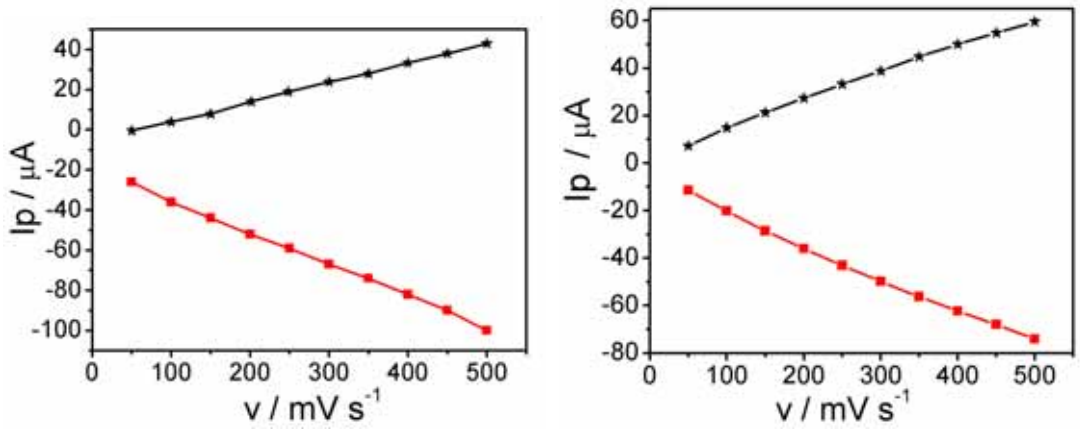

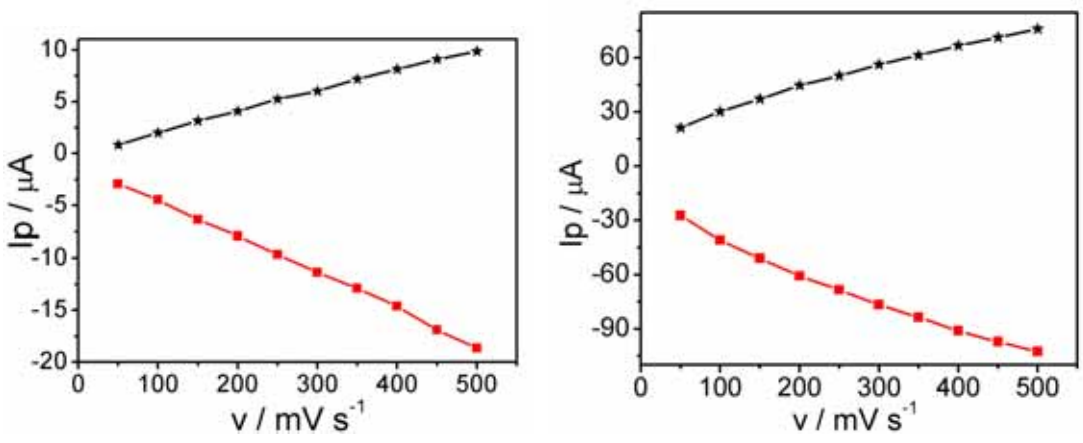

(c) **(d)**

Fig. S9. The plots of the anodic and the cathodic peak II-II' currents against scan rates for the **1**-CPE (a), **2**-CPE (b), **5**-CPE (c), and **6**-CPE (d).

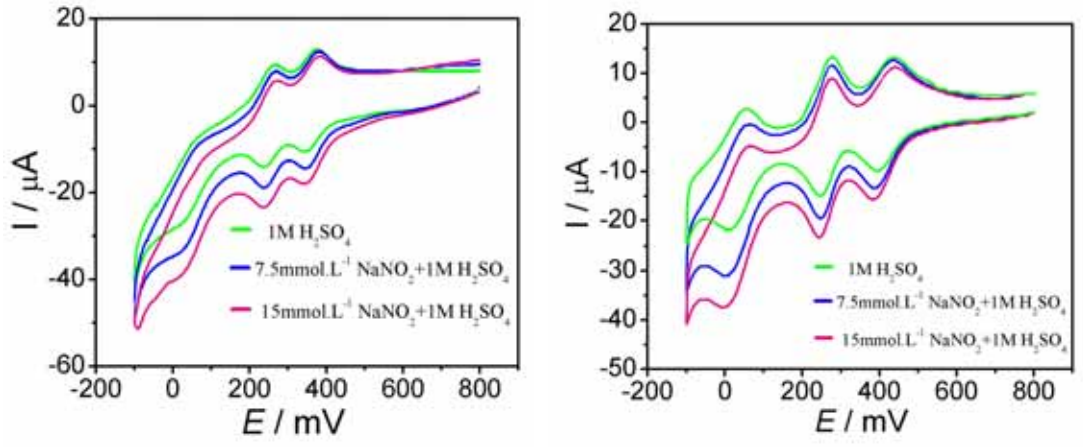

(a) **(b)**

Fig. S10. Cyclic voltammograms of the **2**-CPE (a) and **6**-CPE (b) in 1M H_2SO_4 containing different concentrations of NO_2^-.